Design and Integration of an Air Releasable Autonomous Unmanned Ground Vehicle

Conference Paper · June 2019

DOI: 10.1109/RAST.2019.8767429

5 authors, including:

Mert Çelikol
Yildiz Technical University
1 PUBLICATION **1** CITATION
SEE PROFILE

Ismet Can Hasançebi
Yildiz Technical University
1 PUBLICATION **1** CITATION
SEE PROFILE

Ahmet Kirli
Yildiz Technical University
30 PUBLICATIONS **95** CITATIONS
SEE PROFILE

Design and Integration of an Air Releasable Autonomous Unmanned Ground Vehicle

Faruk Fazlı OKUMUŞ
Depart. of Mechatronics Engineering
Yildiz Technical University
Istanbul, Turkey
farukokumus98@gmail.com

Mert CELIKOL
Depart. of Mechatronics Engineering
Yildiz Technical University
İstanbul, Turkey
mertcelikol@hotmail.com

Ismet Can HASANCEBI
Depart. Of Mechatronics Engineering
Yildiz Technical University
İstanbul, Turkey
ismetcanhasancebi@gmail.com

Mucteba UZUNOGLU
Depart. of Control and Automation Engineering
Yildiz Technical University
İstanbul, Turkey
mucteba.55@gmail.com

Ahmet KIRLI
Depart. of Mechatronics Engineering
Yildiz Technical University
İstanbul, Turkey
ahmetkrl@gmail.com

***Abstract*— In situations where the aircraft has limited capability in accessing to a target point, we can benefit from the cooperation of it with a ground vehicle. This system can be used in applications of many different areas such as space exploration, defense, search & rescue, and commercial delivery. Mostly minimalist mechanical designs that may provide fulfilling certain tasks are pursued in these applications. In this study we focus on developing two main parts of the system through simulations. The airdrop of the Unmanned Ground Vehicle (UGV) to achieve a landing that can guarantee no damage on both the vehicle and the payload and an acceptable range of targeting onto the impact point is studied. Also, upon landing, the control system that can lead the vehicle to have an autonomous drive over an open terrain is designed. The simulation results confirm that the tasks associated with both stages can be conducted in convenience.**

Keywords*— *Unmanned Ground Vehicle, Unmanned Aerial Vehicle, Autonomous driving, Aero breaking

I. INTRODUCTION

UGVs are capable of autonomous drive. There are many kinds of UGVs with some design changes according to their application areas. UGVs have gained importance with the development of unmanned systems. UGV can be used in many areas such as space technologies, transportation, and defense industry. When UGV studies are examined in different fields, it is clearly seen that developments are made by using the same technologies even if the tasks of the vehicles are different. This paper presents some experimental results of an UGV which is constructed for the AUVSI SUAS 19 Competition air drop mission which is to take place in Maryland, USA, annually.

Competitors simulate package delivery to lands UGV cannot reach itself. UGV must drop from the aircraft then the UGV must land on predetermined location and drive autonomously to desired destination. During the whole process UGV and payload, which is 8 oz water bottle, must be prevented from any physical damage. Mission is illustrated in Fig 1.

Earlier researches on mobile robots and autonomous vehicles are done by Flyyne (1985), Klafter (1988), Meystel (1991) and Everett (1995) according to Douglas W. Gage [1]. The major objectives of an UGV is listed as follows; reconnaissance, surveillance, search & rescue with security robots, scientific research with planetary rovers. In these works, the tasks such as image processing, path planning were studied. There are a few studies for dropping the vehicles sent into space.[2]

The main contribution of this paper is the unique design of an UGV meant to be able to travel autonomously to the places where man cannot reach. The UGV is released from an UAV and then fulfills its missions autonomously.

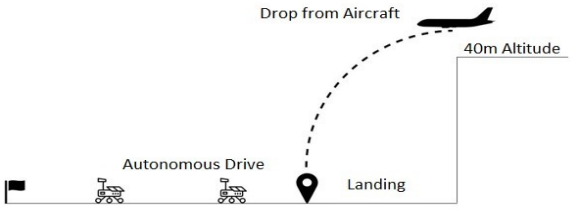

Fig. 1. Summary of Mission

The UGV communicates with the ground station via the telemetry antenna. The vehicle can be controlled with a user interface on ground control station by operators. The designed vehicle has a parachute to reduce the falling speed. When the UGV goes beyond the boundaries specified by the competition, it is planned to stop in fail-safe mode.

This paper includes information about innovative designs and analyses for the UGV in order to meet competition rules. As a result, a robust, innovative and modular real-time UGV is designed, manufactured and assembled.

The rest of this paper is organized as follows. Section 2 describes UGV system overview together with its mechanical design and simulations, followed by manufacturing and the mechanism of dropping. In section 3, modelling the all system combined with designing the controller and its simulations are used to illustrate results how the controller of effects. Finally, conclusion summarizes the obtained outcome of the studies in Section 4.

II. SYSTEM OVERVIEW

A. Mechanical Design and Simulations

The objectives of the mechanical design are to assembly a trigger system to drop the UGV, provide a safe and precise landing. Also, it must autonomously carry the payload inside

it to the given point. For these tasks our UGV had two major limitations. One limitation was that we already had a functional UAV so to properly mount it on the plane needed extra a careful design plan. Second regarding the competition, we had a weight limit of 1,3 kg that should not be exceeded.

Several ideas were thought. A structure for failure design led to exceed weight limit. For a standalone drop, we couldn't design a suspension system enough to absorb the impact energy. So, to accomplish these tasks a parachute design is chosen over a structure to failure or a standalone drop. The complete system works that hereunder our estimation we trigger the drop system. This lets the UGV to a free fall for 0,78 seconds until the parachute is effective. When the parachute is deployed the UGV will get slowed to a speed of 4 m/s. See (1), (2), (3). With the help of an altitude meter the altitude is measured and about 1 m above the ground the separation with the parachute system is triggered. After the touchdown the UGV will drive to the given destination in the shortest time possible.

Firstly, analysis and simulations were made for the drop of the UGV. Solidworks Simulations was used mainly for Explicit Dynamics. This analysis was run with the condition of a 4 m/s touchdown speed. According to the Drop simulation in Fig. 2 it will get a maximum stress of 166,1 MPa. This value doesn't exceed the mechanical properties of the chosen carbon fiber.

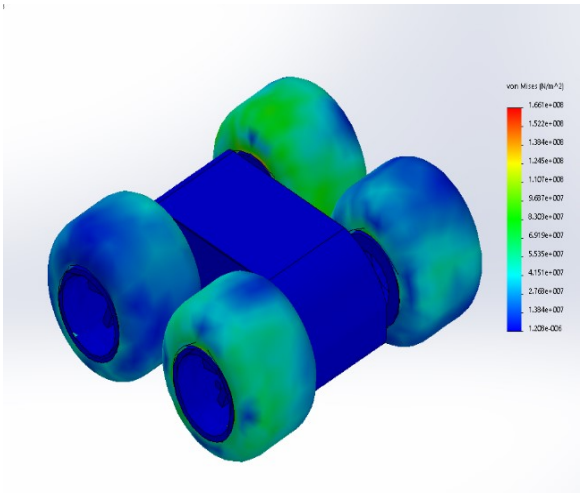

Fig. 2. Drop Simulation of UGV in Solidworks

Equation (1) calculates the time of the separation above 1 m of impact. The second equation evaluates the touchdown speed of the UGV. The final equation gives the impact energy.

$$\frac{1}{2}.\,a\,.\,t^2 = x \tag{1}$$

$$V_f = V_i + a.t \tag{2}$$

$$W_{total} = \frac{1}{2}.m.V_f^2 \tag{3}$$

Even though the material of the body could resist the impact a damping system is designed to help to absorb the impact and make it easier to drive in rugged environments. DC motor mounting bracket and 3D printed ABS parts were used Fig. 3.

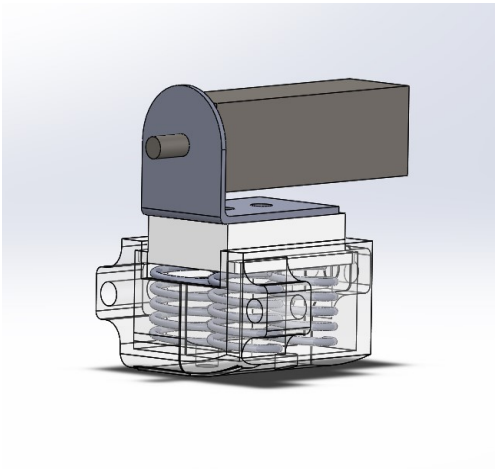

Fig. 3. Suspension system of the motor

Each assembly has 4 springs in series connection. That makes 16 springs in total. The spring constant and the energy which springs can absorb is calculated according to Hook's Law [3] shown in (4), (5).

$$F = k.\,x \tag{4}$$

$$\frac{1}{2}.(16.k)\,.x^2 \qquad [3](5)$$

To drop the UGV a special trigger system was designed for our needs. It had to be rigid enough to withstand any turbulence during the flight, easy detachable and to release the payload without any delay in separation. A two-step separation was planned as shown in Fig. 4. When the servo on the fuselage is triggered the UGV and the parachute are released from the UAV. The second step is to trigger the second servo on the UGV to release the parachute.

B. Drop Mechanism

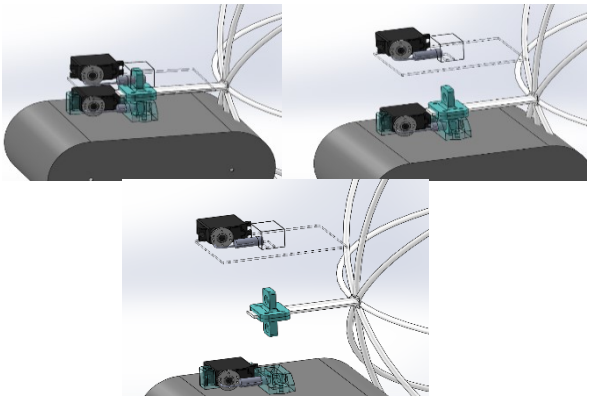

Fig. 4. Top Left: Airdrop trigger system is locked. Top right: Release of the UGV and the parachute Bottom: Detach of the parachute.

C. Parachute Design and Calculations

The parachute was designed according to the wanted speed of the UGV. The formula (6) was used to calculate the necessary area.

$$S = \frac{2.m.g}{R.C_x.V^2} \tag{6}$$

TABLE I. NOTATION OF PARACHUTE

R	Air Density (For Sea level: 1,225 kg/m³)
S	Parachute Area
C_x	Drag Coefficient
V_0	Speed
M	Weight
g	Gravity (9,81 m^2/s)

The parachute dimensions are shown in the Fig. 5. An area of 0,917 m^2 necessary with a Cx of 1,2 [4].

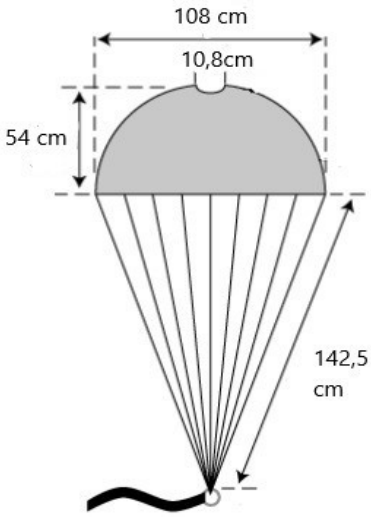

Fig. 5: Parachute Design

When the parachute is deployed a force will act on the surface due to the drag, see (7).

$$F = \frac{R.S.C_x.V_0^2}{2} \quad (7)$$

To analyses the impact on the cover of the UGV when the parachute is deployed. A static force simulation was made on Solidworks see Fig. 6. With a deformation under 0.03 mm the force on the release can be neglected.

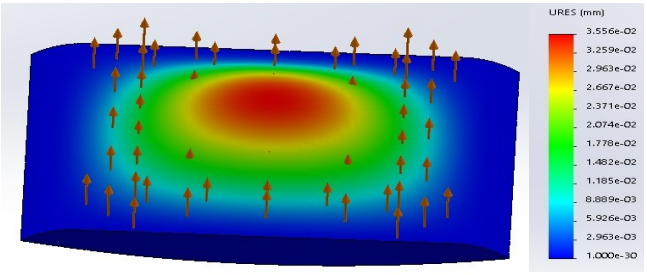

Fig. 6. Parachute experimental result

A representative weight equivalent to UGV which has an accelerometer and barometer in its was parachuted from a height of 18 meters. The speed of the vehicle was logged versus to the height as shown in the Fig. 7 After a 2.8 m descend the parachute opened and slowed the UGV to a constant speed of 4.5 m/s.

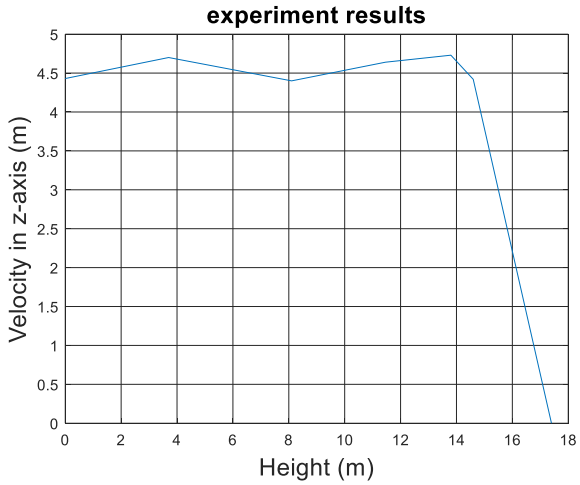

Fig. 7. Speed to height graph of the parachute

D. Motor Selection

The UGV needs to drive properly on rough surfaces such as grass. Also, the motors need enough torque to support the vehicle. For this the needed calculations are as follows (8), (9), (10), (11), (12), (13).

TABLE II. VEHICLE PROPERTIES

Ground vehicle weight (GVW)	1 kg
Weight on each wheel (W_w)	0.275 kg
Radius of wheels (R_w)	0.096 m
Maximum incline angle (α)	2 deg
Desired top speed	10.8 km/h
Desired acceleration	5 m/s^2
Worst working surface (Grass)	0.55
Soft Rubber on dry concrete (μ)	0.85
Resistance Factor (RF)	1.1
Distance between motor shaft and wheel (DBMSW)	0.025 m

To calculate the total tractive effort (TTE) the parameters on (8) are needed.

$$TTE = RR + GR + F_a \quad (8)$$

Rolling resistance (RR) because of the rough surface is calculated in (9).

$$RR = W_{GV}.C_\pi \quad (9)$$

Grade resistance (GR) when climbing a terrain that is not plain is calculated in (10).

$$GR = W_{GV} . \sin\alpha \quad (10)$$

Acceleration force (F_a) is the force when the UGV accelerates from an initial position. It is calculated in (11).

$$F_a = \frac{W_{GV}.V_{max}}{g.t_a} \quad (11)$$

With the result of the calculations above the wheel motor torque (Tw) can be calculated as shown in (12).

$$T_W = TTE.R_w.RF \quad (12)$$

To compare the theoretical result with a reality, check the maximum tractive torque (MTT) is calculated in (13).

$$MTT = W_w.\mu.R_w \quad [5] \quad (13)$$

From these calculations we conclude in (14), (15) that the UGV will not slip and he motors will generate enough torque to drive the motors for the given circumstances.

$$T_w < MTT \,.\, 4(\text{Drive Wheel Number}) \quad (14)$$

$$TTE.(DBMSW) < \text{MotorNominalTorque} \quad (15)$$

E. Computational Fluid Dynamics(CFD) Analysis

To hit the target with a better accuracy a CFD analysis was performed on half of a simple 3D model of the UGV. According to the results times two, the drag coefficient (Cd) of 0.5762 was calculated see Fig. 8. This parameter was used in the airdrop algorithm to determine the release moment of the payload.

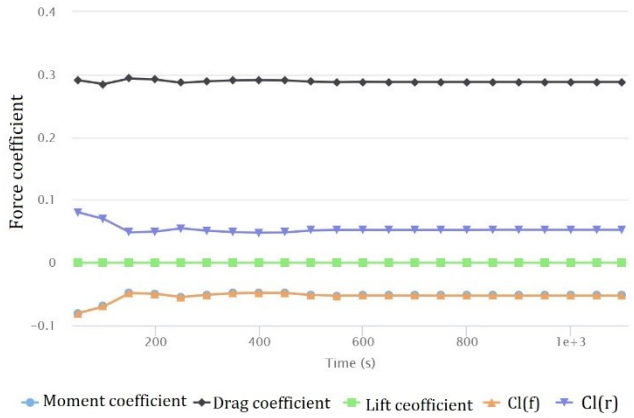

Fig. 8. CFD analysis of the UGV in SimScale

A render of the mechanical system of the UGV is showed with the parachute in Fig. 9.

Fig. 9. Final render of UGV

III. Modeling the System and Designing Controller

A. Modelling of the System

To find a model of the UGV, some assumptions were accepted[9]. We assume that the vehicle moves in 2-D plane and wheels are in permanent contact with the flat surface. We also assume that slip and skid forces between the tires and flat surface do not change with position.

Dynamic model of the mobile platform was derived by using Lagrange Method. The model and the controllers of the nonholonomic mobile robot was implemented by using MATLAB/Simulink.

Kinematic based backstepping controller was used and designed based on waypoint tracking algorithms. For each DC motor, PID Controller was used.

For each DC motor, PID Controller was used. Each symbol in figures and equations listed below represents as follows.

TABLE III. NOTATIONS FOR EQUATIONS

V_1	Local velocity of the UGV perpendicular to axle
V_2	Local velocity of the UGV parallel to axles
$V_{R,L}$	Circumferential velocities of the wheels
φ	Course angle of the platform
R	Radius of the wheels
$2L$	Wheelbase
M	Mass of the platform
J	Moment of inertia of the platform
x, y	Coordinates of the current pose of UGV
$\tilde{x}, \tilde{y}$	Coordinates of the destination
D	Distance between Center of Gravity (CG) and Geometric Center (GC)

B. Kinematics of UGV

The platform is considered as system of rectangular shape rigid body see Fig. 10. Motion of the platform is calculated with respect to inertial frame XY. For modelling purpose, we suppose that the platform is geometrically symmetric also center of gravity CG is on the geometric center GC of the platform. Position of the vehicle with respect to the inertial frame is given by x y coordinates of CG and by angle of ϕ.

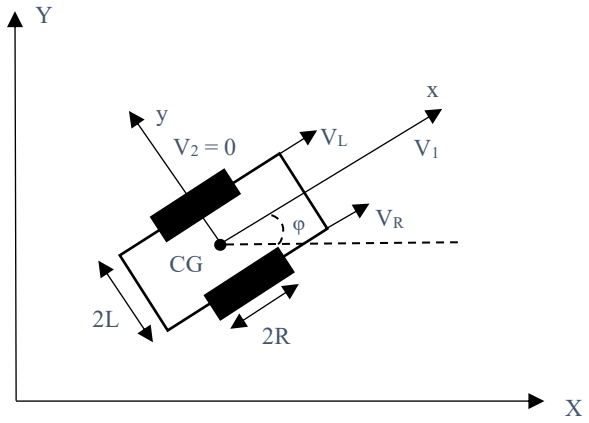

Fig. 10. Generalized Coordinates

In this model there are 4 DC motor for each wheel. Motors on the same side do the same job so for sake of simplicity assumed that two motors were used. This model can describe by using (16), (17), (18) [9].

$$V_1 = \frac{V_R+V_L}{2} \tag{16}$$

$$V_2 = 0 \tag{17}$$

$$\dot{\varphi} = \frac{V_R+V_L}{2} \tag{18}$$

Also derived global velocities of the mobile platform by using (19), (20) [9].

$$\dot{x} = V_1.\cos\varphi - V_2.\sin\varphi \tag{19}$$

$$\dot{y} = V_1.\sin\varphi + V_2.\cos\varphi \tag{20}$$

After these equations block, integrate global values and get the pose values of the differential drive mobile robot. In Figure 11. Flow chart of the mobile platform from velocities of the wheels to global position of the differential drive robot is shown. In model, masses and forces must be considered so this result is dynamic model of the mobile robot.

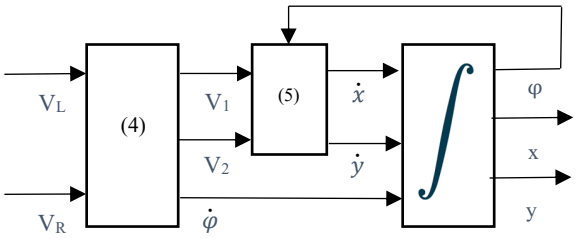

Fig. 11. Block Diagram of the Kinematic Model

C. Dynamics of UGV

In kinematic models, dynamics of the system are neglected. For represent actual motion of the differential drive mobile robot, it is important to derive dynamic model of the platform [9].

For deriving the dynamic model, there are 2 methods. Newton-Euler method describes the system in terms of all the forces and momentum acting on the system based of direct interpretations of Newtons Second Law of Motion [11].

On the other hand, Lagrange method incorporates the concepts of Work and Energy to indirectly derive the equations of motion. Here, Lagrange method is chosen due to its more systematic nature and automatic elimination of workless and constraint forces [11].

Lagrange Approach for Dynamics Modeling

Lagrange approach used potential and kinetic energy to derive equation of motion and is given in (21).

$$\frac{d}{dt}\left(\frac{\partial L}{\partial \dot{q}_i}\right)+\frac{\partial L}{\partial q_i}=F-\Lambda^T(q)^\lambda \tag{21}$$

By using Lagrange approach, (22), (23) easily can be derived**.** Those equations show the actuator torques applied to the wheels

$$M\dot{v}_1-MD\ddot{\theta}\dot{\theta}=\frac{1}{R}(\tau_R+\tau_L) \tag{22}$$

$$(MD^2+J)\ddot{\theta}+MDv_1\dot{\theta}=\frac{L}{R}(\tau_R-\tau_L) \tag{23}$$

These two equations which are represent Dynamical behavior of the platform can be shown in steady-state matrix form is shown in below [11]**.**

$$\begin{bmatrix} M & 0 \\ 0 & MD^2+J \end{bmatrix}\begin{bmatrix} \dot{v}_1 \\ \ddot{\theta} \end{bmatrix}+\begin{bmatrix} 0 & -MD\dot{\theta} \\ MD\dot{\theta} & 0 \end{bmatrix}\begin{bmatrix} \dot{v}_1 \\ \ddot{\theta} \end{bmatrix}=\frac{1}{R}\begin{bmatrix} 1 & 1 \\ L & -L \end{bmatrix}\begin{bmatrix} \tau_R \\ \tau_L \end{bmatrix} \tag{24}$$

D. Modeling Actuator

For UGV system, armature-controlled Dc motors used as actuator. Armature voltage V_A is used as control input. Following (25), (26), (27), (28) can be easily obtain from Figure 12**.** for permanent magnet DC motors (PMDC).

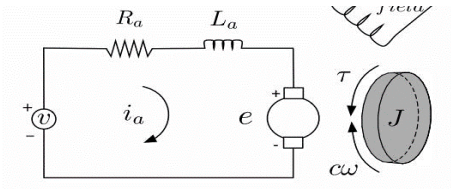

Fig. 12. Circuit of the DC motor

$$v_a = R_a.i_a+L_a.\frac{di_a}{dt}+e_a \tag{25}$$

$$e_a = K_b.\omega_m \tag{26}$$

$$\tau_m = K_t.i_a \tag{27}$$

$$\tau = N.\tau_m \tag{28}$$

Skid-steer system take the torques of left and right motors (τ_L, τ_R) and give output left and right wheels angular velocity. Block diagram of the vehicle dynamic is shown in Figure 13.

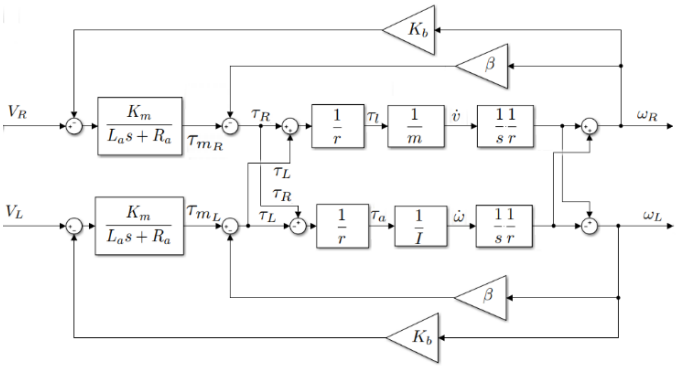

Fig. 13. Block diagram of the UGV dynamics [10]

E. *Designing the Controller*

In this paper two different type of controller used for motion tracking of UGV platform. To design a controller, MATLAB/Simulink platform was used. All system was conducted gradually on simulation.

1) Actuator Controller

First, vehicle dynamics were simulated and DC motors rotational speeds on each side were controlled by PID controller. To set the coefficients K_p, K_i, *and* K_d of the controller, Ziegler–Nichols method was used. To construct the transfer function, data about the motor obtain from datasheet. Properties of the DC motor shown in Table 4.

TABLE IV. PROPERTIES OF THE DC MOTOR

Symbol	Parameter	Value	Unit
M	Mass	1.3	Kg
J	Inertia	0.0551	$Kg.m^2$
L_a	Armature Inductance	$0.64x10^{-3}$	H
R_a	Armature Resistance	0.27	Ohm
K_b	Back EMF Constant	0.048	V/(rad/s)
K_T	Torque Constant	0.048	N.m/Amp
β	Friction Constant	0.71	N.m.s
R	Wheel Radius	48.26	Mm
L	Wheelbase	0.118	M

2) Motion Controller

Waypoint tracking control by using kinematic based backstepping controller. This logic is only taking criterion distance and angle between current position and destination point by using (29), (30).

$$d = \sqrt{(\bar{y}-y)^2+(\bar{x}-x)^2} \quad (29)$$

$$\Phi = \tan^{-1}\frac{\bar{y}-y}{\bar{x}-x} \quad (30)$$

Motion controller do proportional control on $\dot{\varphi}$ as shown in (31). In this control, 1.7 was taken as proportional coefficient of controller. For design parameters, V_1= 0,5 m/s was given.

$$\dot{\varphi} = \Phi(1,7)(K_p) \quad (31)$$

For simulate these conditions, flow chart was used to build motion controller algorithm. When U.G.V reach the waypoint, algorithm check whether it is destination or not. if it is not a final waypoint, pass to next waypoint in queue. All system is shown in Fig. 14. in Simulink.

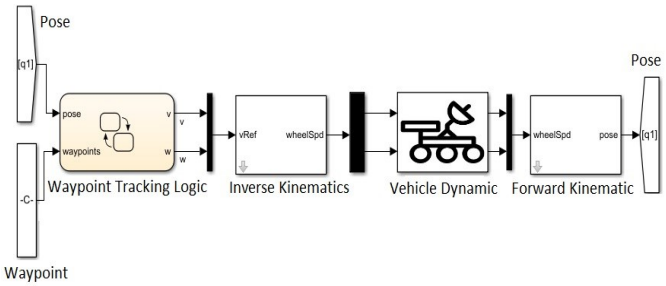

Fig. 14. All UGV system is simulated as block diagram in Simulink.

F. *Validation*

The proposed method is validated with the skid-steer vehicle through experiments. Results of the experiments and the experimental setup are presented. Then, simulations and experiments are discussed. Simulation time was selected as T= 50 s.

1) Experimental Setup

The weight of the vehicle is 1.3 kg, and the width and lengths are 170 mm and 150 mm. On-board processor which is ARM cortex-M4 STM32F4 with up to 180 MHz operating frequency calculates the control input. The pose of vehicle is obtained with GPS and magnetometer. The control system is simulated in MATLAB-Simulink.

To validate the performance of the autopilot, the experiment is conducted on a rectangular path. The results of the simulations are compared with the results of the experiments as shown in the Fig. 15.

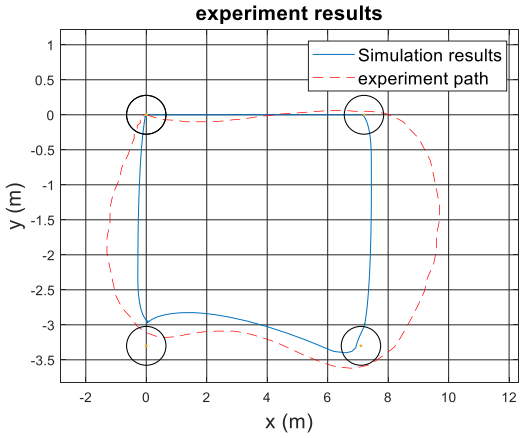

Fig. 15. Path results of experimental and simulation are compared

CONCLUSION

In this study, a UGV that fulfills the requirements of the AUVSI SUAS competition is designed and manufactured. The UGV with a payload is released to a pre-determined point from the aircraft without any damage to payload. Then, UGV delivers the payload to another determined point. The presented UGV has several innovative properties. The mechanical design and the parachute system are developed in order to get the vehicle and payload to their destination safely. Backstepping controller is applied to path tracking control for

skid-steer vehicle. To drive effectively, the cost formulation is selected as the one which combines the speed regulation and the path following. Test results show that this approach can attain highly effective performance

REFERENCES

[1] D. W. Gage, "Special Issue on Unmanned Ground Vehicles FIGURES OMITTED Unmanned Systems Magazine," vol. 13, no. 3, 1995.

[2] F. Abilleira, "2011 Mars Science Laboratory trajectory reconstruction and performance from launch through landing," *Adv. Astronaut. Sci.*, vol. 148, pp. 487–503, 2013.

[3] A. P. Tipler and G. Mosca, *Physics for scientist and engineers*. 2004.

[4] T. W. Knacke, *Parachute Recovery Systems*. 1991.

[5] C. Surface, "EML2322L – MAE Design and Manufacturing Laboratory Drive Wheel Motor Torque Calculations Reference Citation: White Hydraulics Drive Products," vol. 01, pp. 5–6.

[6] H. K. Celik, A. E. W. Rennie, and I. Akinci, "Deformation behaviour simulation of an apple under drop case by finite element method," *J. Food Eng.*, vol. 104, no. 2, pp. 293–298, 2011.

[7] L. Le, D. Rosa, A. Gracia, D. Barranco, and L. Rallo, "Fatty acid composition of advanced olive," vol. 1926, no. April, pp. 1921–1926, 2008.

[8] *Paul M Kurowski - Engineering Analysis with SOLIDWORKS Simulation, 2018*.

[9] F. Solc and J. Sembera, "Kinetic model of a skid steered robot," *Proc. 7Th Wseas Int. Conf. Signal Process. Robot. Autom. Adv. Top. Signal Process. Robot. Autom.*, pp. 61–65, 2008.

[10] I. Anvari," *Non-holonomic Differ. Drive Mob. Robot Control Des. Crit. Dyn. Coupling Constraints*, vol. 84, no. November, pp. 487–492, 2013.

[11] R. D. Ahmad Abu Hatab, "Dynamic Modelling of Differential-Drive Mobile Robots using Lagrange and Newton-Euler Methodologies: A Unified Framework," *Adv. Robot. Autom.*, vol. 02, no. 02, 2013.

[12] B. Diriba, H. Prof, and W. Zhongmin, "Design and Control for Differential Drive Mobile Robot," vol. 6, no. 10, pp. 327–335, 2017.

[13] G. Songul *et al.*, "Model picosatellite design for energy harvesting and telemetry data transmission through RF communication," *RAST 2015 - Proc. 7th Int. Conf. Recent Adv. Sp. Technol.*, pp. 839–844, 2015.

[14] S. N. Bulut *et al.*, "Model satellite design for CanSat Competition," *RAST 2013 - Proc. 6th Int. Conf. Recent Adv. Sp. Technol.*, pp. 913–917, 2013